THE ROYAL SOCIETY

Published online 12 August 2003

Comparing fluid mechanics models with experimental data

G. R. Spedding

Department of Aerospace and Mechanical Engineering, University of Southern California, Los Angeles, CA 90089-1191, USA (*geoff@usc.edu*)

The art of modelling the physical world lies in the appropriate simplification and abstraction of the complete problem. In fluid mechanics, the Navier–Stokes equations provide a model that is valid under most circumstances germane to animal locomotion, but the complexity of solutions provides strong incentive for the development of further, more simplified practical models. When the flow organizes itself so that all shearing motions are collected into localized patches, then various mathematical vortex models have been very successful in predicting and furthering the physical understanding of many flows, particularly in aerodynamics. Experimental models have the significant added convenience that the fluid mechanics can be generated by a real fluid, not a model, provided the appropriate dimensionless groups have similar values. Then, analogous problems can be encountered in making intelligible but independent descriptions of the experimental results. Finally, model predictions and experimental results may be compared if, and only if, numerical estimates of the likely variations in the tested quantities are provided. Examples from recent experimental measurements of wakes behind a fixed wing and behind a bird in free flight are used to illustrate these principles.

Keywords: bird flight; aerodynamics; aerofoil wakes; uncertainty analysis

1. PROLOGUE

This paper starts with quite general remarks on the philosophical basis for making models. In so doing, certain aspects of the introductory remarks by Alexander (2003) will be amplified and placed in sharper relief for the following examples in the particular field of experimental fluid mechanics. The paper is thus somewhat unusual, veering between the general and specific. Both are deliberately strongly selected. The general comments are more broad than usual, and some of the modelling details are discussed in much more fine grain than is customarily given outside discipline-specific texts. The purpose of the paper is to illustrate the relationship between the two, and also to deliberately illuminate aspects of the modelling enterprise often omitted or taken for granted. So, this is not a review, nor even an overview. It is a view of how models, particularly fluid mechanics models, can be made and tested. In its selectivity, it is hoped that the material might be digested and remembered as a whole, and even that the specific lessons drawn and summarized in the final section might be acted upon.

2. THE ART OF MODELLING

(a) *What kind of model?*

A model (of any kind) can only be designed and implemented if its purpose is specified explicitly and clearly. This is essential not only for its construction, but also for testing and evaluation. Let us denote this as the objective set, O. Success or failure of a model is then defined exclusively in terms of O. Here, we will implicitly assume two quite common purposes in science and engineering:

(i) to further (broaden or deepen) understanding of a physical phenomenon; and
(ii) to make testable predictions about it.

In general, we look for some model, M, that satisfies

$$M \approx P, \tag{2.1}$$

where P is the physical system of interest. The 'almost equal to' sign is used to denote the fact that, by definition, M is *not* equal to P, but according to the original purpose statement, it acts close enough to it. To be most general, let P now represent the physical universe, and M the set of all possible models.

The different types of modelling approach to understanding the universe are shown in figure 1. In figure 1*a*, $M \not\subset P$, a distressingly common situation exemplified, for example, by belief in UFOs, astrology, ESP and so on. Slightly more common is figure 1*b* where there is partial overlap between M and P. Most of us are quite comfortable in simultaneously having various conceptual models occupying either part. A quantitative testable model that specifically aims to apply to P (as stated in O) must apparently occupy some region like figure 1*c*, where its reach is constrained by the actual physical universe, P. This seems reasonable since it is P that we wish to model. The remaining task appears to be to select the part of P that appears in M.

One contribution of 20 to a Theme Issue 'Modelling in biomechanics'.

DOI 10.1098/rstb.2003.1352

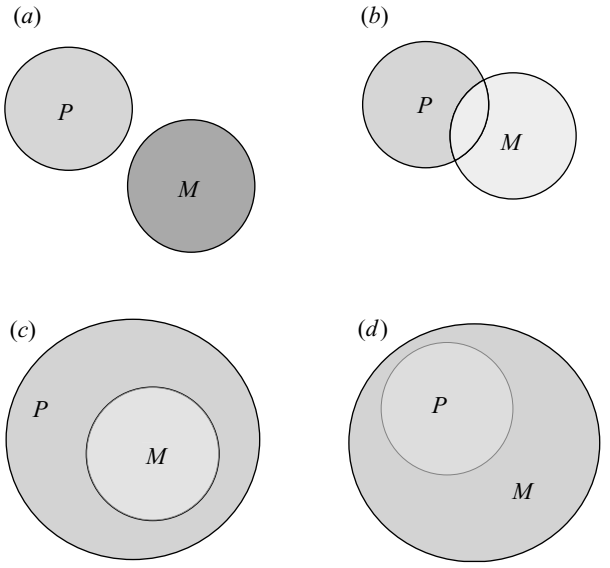

Figure 1. Four different possible relationships between mathematical (or other) models, *M*, and the physical universe, *P*. There may be (*a*) no, (*b*) partial, or (*c*,*d*) complete overlap. Useful models (*M*) might be completely constrained by *P*, as in (*c*), but part of the art of modelling comes in relaxing this constraint and deliberately allowing *M* to stray outside *P*. This can be justified on grounds of increased simplicity, clarity, elegance or even convenience. The success or validity of a model is actually judged only in terms of separately defined objectives, *O*.

In fact, a useful model need not be constrained by *P*, and can be drawn from the larger pool of available models shown in figure 1*d*. Certain features can be deliberate distortions of reality. Here, an analogy may be drawn with painting in Chinese Zen Buddhism, where the omission of matter is as important as the presence of it, and where sparse economy of line and shade is valued highly.[1] So it is with most successful mathematical models of the physical universe. Economy, simplicity and clarity of representation can supersede the requirement for fidelity. The complete omission of some can be justified in the name of increased elegance, convenience, simplicity, and so the remaining features are exaggerated in importance. Even these can be deliberately modified, apparently to taste.

How then, can we distinguish useful mathematical models of physics if physics itself cannot be used as a criterion for judging them? The short answer is a reminder that the performance of the model need be justified *only* in terms of its purpose, *O*, and then, to be considered a scientific model, it must be testable (Popper 1959). Then, and only then, do we have a closed loop in which a model is set up and evaluated, refined and re-evaluated. Strictly speaking, at no time need the model refer to factors outside *O*. A mathematical model can cheerfully disregard aspects of physical reality that are judged to be either superfluous or simply inconvenient. The rigorous selection of material in *M* serves to keep the model tractable, and to make it useful with respect to *O*. This is the necessary and sufficient condition.

Here, one might usefully draw a distinction between modelling and simulation. The latter typically incorporates as many realistic elements as required to satisfy *O*. If the model fails the test, then more elements are added to increase the degree of realism, or the assumptions in existing components are made more realistic and usually more complex. Such is not necessarily the case in general modelling. Elements can be quite creatively and wilfully unrealistic, provided the overall objective is served. Some corollaries of this rather startling situation can cause confusion or even alarm. For example, the fact that a mathematical or physical model is at the outset verifiably incorrect (in terms of strict physical accuracy) need not necessarily prohibit or inhibit its use. An example will be found in § 4.

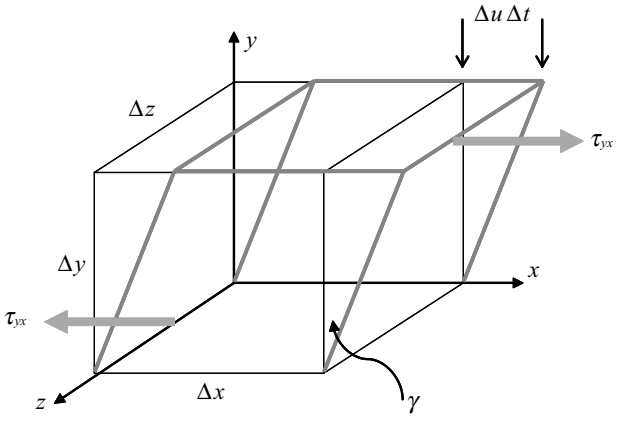

Figure 2. The response of a fluid element to shear stress in one direction. The initially cubical volume is subject to shearing motion so that the top face moves horizontally (relative to the bottom) by a distance $\Delta u \Delta t$.

3. MATHEMATICAL–PHYSICAL ($M \subset P$) MODELS

Here, we will illustrate and explain the principles and selected details of the model equations that form the foundations of modern fluid mechanics in general, and aerodynamics in particular.

(a) *Physical properties of a fluid element*

An essential component of fluids modelling is the fluid element, shown in figure 2. The fluid element is an imaginary object of size Δx, Δy, Δz, where there are enough molecules inside the volume so that it may be considered a continuum, but the volume is sufficiently small so that all physical properties are uniform within it. If the fluid element is subjected to a shearing motion due to a uniform gradient of u in y, the fluid is deformed as shown in the heavy lines of figure 2. This is, after all, the definition of a fluid: a substance that will assume the shape of a container into which it is introduced. If we imagine that the shearing motion is applied in one direction only, by something (neighbouring fluid elements or a solid surface) moving with speed Δu at the top with respect to zero at the bottom, and over a time Δt, then simple trigonometry relates change in strain angle, γ, with the strain in x, $\Delta u \Delta t$, by

$$\Delta u \Delta t = \Delta y \sin \Delta \gamma. \tag{3.1}$$

For small $\Delta \gamma$, $\sin \Delta \gamma \approx \Delta \gamma$, and equation (3.1) can be rearranged to give

$$\frac{\Delta\gamma}{\Delta t}=\frac{\Delta u}{\Delta y}. \tag{3.2}$$

For small increments, the strain rate, $\mathrm{d}\gamma/\mathrm{d}t = \mathrm{d}u/\mathrm{d}y$, and for Newtonian fluids, the shear stress in the x direction owing to gradients in y for the particular case of figure 2 is the product of a constant viscosity, μ, with the strain rate

$$\tau_{yx}=\mu\frac{\mathrm{d}u}{\mathrm{d}y}. \tag{3.3}$$

The fluid viscosity, μ, represents the comparative resistance to deformation. The higher the value of μ, the smaller the strain rate for a given stress. It is analogous, in some respects, to the shear modulus for a solid, but it multiplies the strain *rate*, not the strain. If μ is high, a significant amount of energy is required to overcome internal resistance to deformation (internal friction) within some fixed time interval. Fluids are, in general, characterized by their extremely *low* resistance to deformation, and it is simply a matter of how long it takes to occur.

Many biofluids do not behave much like equation (3.3). However, for the particular case of locomotion, the fluid in which the animal is immersed is usually either water (fresh or sea) or air, and both of these are quite well modelled by equation (3.3).

(b) *Newtonian fluids*

(i) *The physical basis for the equations of motion of a moving fluid*

As eloquently explained by Pennycuick (1992), Newton's laws are quite sufficient to explain most phenomena encountered in biomechanics. We may therefore begin with the fluid element model and its result in equation (3.3). Newton's second law can be taken as unproblematic

$$F=ma, \tag{3.4}$$

and it states that, for a moving object, the force, F, experienced by that object is a product of its mass, m, and acceleration, a. This expression can be written more informatively as,

$$\boldsymbol{F}=\frac{\mathrm{d}}{\mathrm{d}t}(m\boldsymbol{V}), \tag{3.5}$$

where $\boldsymbol{F}$ and $\boldsymbol{V}$ are vector quantities and the equivalence of force as rate of change of momentum is clear. When this equation is applied to a fluid modelled as in figure 2, we arrive at an equation describing how forces are balanced in a continuous fluid

$$\rho\frac{\mathrm{D}\boldsymbol{V}}{\mathrm{D}t}=-\nabla p+\rho\boldsymbol{g}+\mu\nabla^2\boldsymbol{V}. \tag{3.6}$$

Physical interpretation can be made for each term. On the left-hand side, $\mathrm{D}\boldsymbol{V}/\mathrm{D}t$ is the local time derivative of the vector velocity, $\boldsymbol{V}$, so it is an acceleration, with direction. It is multiplied by the density, which is mass per unit volume, and so combined they represent the local force over a unit volume of fluid—conceptually the same volume as introduced in figure 2. The first term on the right-hand side is the spatial gradient in pressure. The leading minus sign states that positive pressure gradients oppose the acceleration—when the pressure in a given direction increases, the fluid element travelling in that direction decelerates. Frequently, the remaining two terms are comparatively small, when a simple physical interpretation of the reduced equation

$$\boldsymbol{F}=\rho\frac{\mathrm{D}\boldsymbol{V}}{\mathrm{D}t}=-\nabla p, \tag{3.7}$$

is that fluid accelerations, and hence forces, can be generated and opposed *only* by pressure gradients.

Back at the full equation (3.6), the middle term on the right-hand side is the local gravitational force. If neither $\boldsymbol{g}$ nor ρ change very much over the problem domain (this is usually true), then this force component is constant everywhere and can be ignored. The last term gives the contribution of viscous forces. The Laplacian operator, ∇^2, is a measure of the variation in spatial gradients and is multiplied by the local velocity vector. Note how the viscous force acts in opposition to the pressure gradients. While negative pressure gradients cause accelerations of fluid elements, viscosity slows them down.

Equation (3.6) is called the momentum equation, and follows directly from application of Newton's second law (equation (3.4)) to a continuous, incompressible fluid. Just by itself, it does not provide sufficient information on which of the myriad possible combinations of ρ, V, p, $\boldsymbol{g}$ and μ satisfying equation (3.6) will be physical solutions that can occur ($M \in P$, recalling the notation of § 2). Two further well-known physical principles can be invoked, adding additional constraints to the possible solutions. These are the laws of conservation of mass and conservation of energy. Together with equation (3.6) they comprise the renowned Navier–Stokes (NS) equations. Their physical foundation is so solid (Newton's second law + conservation laws) that their physical correctness or applicability is rarely in doubt, provided equation (3.3) can be shown to be reasonable.

Although the vector notation of equation (3.6) may seem to make it inaccessible and hard to relate to physical problems, it is not so hard to expand out to components in Cartesian coordinate systems and cubical fluid elements like figure 2. Here is the x-momentum equation, for example (dropping the gravity term):

$$\rho\frac{\mathrm{D}u}{\mathrm{D}t}=-\frac{\partial p}{\partial x}+\frac{\partial\tau_{xx}}{\partial x}+\frac{\partial\tau_{yx}}{\partial y}+\frac{\partial\tau_{zx}}{\partial z}. \tag{3.8}$$

The τ_{ij} components are just the shear stresses decomposed in the principle directions, and the complete expression for τ_{yx}

$$\tau_{yx}=\tau_{xy}=\mu\left(\frac{\partial u}{\partial y}+\frac{\partial v}{\partial x}\right), \tag{3.9}$$

can be compared with the (only slightly) more simple case of deformation exactly parallel to x given in figure 2 and leading to equation (3.3).

The main point is that although these equations may at first appear formidable, they are in fact quite simple in formulation, and frequently a physical interpretation of individual terms is possible.

(ii) *Complexity of solutions and simulation*

On reflection, it may seem extraordinary that such simple model equations can describe so many fluid flows, which we know from experience can be complicated and

unpredictable. And this is the problem. For, despite their elegance and simplicity, the Navier–Stokes equations can have solutions that are enormously intricate. Very few closed-form (analytical) solutions are known, and these are for special cases (simple geometries, low speeds and special symmetries) that are so simple that they have very restricted application.

The partial differential equations can indeed be integrated numerically to provide solutions for the velocity components u, v and w, together with the pointwise quantities, pressure, p, and density, ρ, as a function of x, y and z. There are three points about this approach (DNS), as noted in general in § 1. First, as the solutions are intricate and complex, then the numerical solutions must be performed with great care, and become very much more complicated to perform as the geometry becomes more complex, and as the Reynolds number (discussed in § 3b(iii)) increases. Second, to have sufficient resolution in space and in time, the DNS of a very large range of practical problems is not feasible on any currently available computer, and is prohibitively expensive for many more. Third, even if plausible solutions are arrived at, we have not necessarily learned anything by merely confirming that the NS model works for this fluid flow—this is the model we prescribed in the first place! Repeated runs of the working solution may well allow an exploration of parameter space that cannot easily be accomplished any other way, but increased physical insight will not necessarily follow.

(iii) *Dimensional analysis*

Dimensional analysis of the Navier–Stokes equations reveals one further important point. The Buckingham–Π theorem states that systems of dimensionally homogeneous equations (e.g. if one term represents a force, then all terms must have dimensions of force) can be recast in terms of dimensionless groups (Π products) whose number is

$$N_\Pi = N_V - N_D, \tag{3.10}$$

where N_V is the number of independent variables and N_D is the number of fundamental dimensions.[2] For a body of characteristic size, D, moving at speed V, then, ignoring the possible contribution from variations in $\boldsymbol{g}$, the independent variables in equation (3.6) are D, V, ρ and μ. As in most fluid mechanics problems, the fundamental dimensions are those of length, L, time, T and mass, M. Thus, $N_\Pi = 4–3$, and one dimensionless group can be used to rescale the equations. The most fundamental of the various dimensionless numbers encountered in fluid mechanics is the Reynolds number, Re, which can be written directly in terms of the independent variables listed:

$$Re = \frac{\rho V D}{\mu}. \tag{3.11}$$

As the equations can be rescaled in this form, then flows where Re is the same are guaranteed to be dynamically similar. The balance of forces will be identical. The balance of forces expressed by equation (3.11) is the ratio of inertial to viscous forces. Geometrically similar bodies of size D immersed in a uniform flow of speed V have identical solutions of the equations of motion if Re has the same value. This is a necessary and sufficient condition. The practical and theoretical implications of this result are very wide ranging. Here, we can immediately note that it suggests a procedure for theoretical and physical modelling, where values of all or any of the independent variables, D and V governing the body size and motion, and also ρ and μ describing the physical characteristics of the fluid, can be manipulated at will. If Re is the same, then so is the flow.

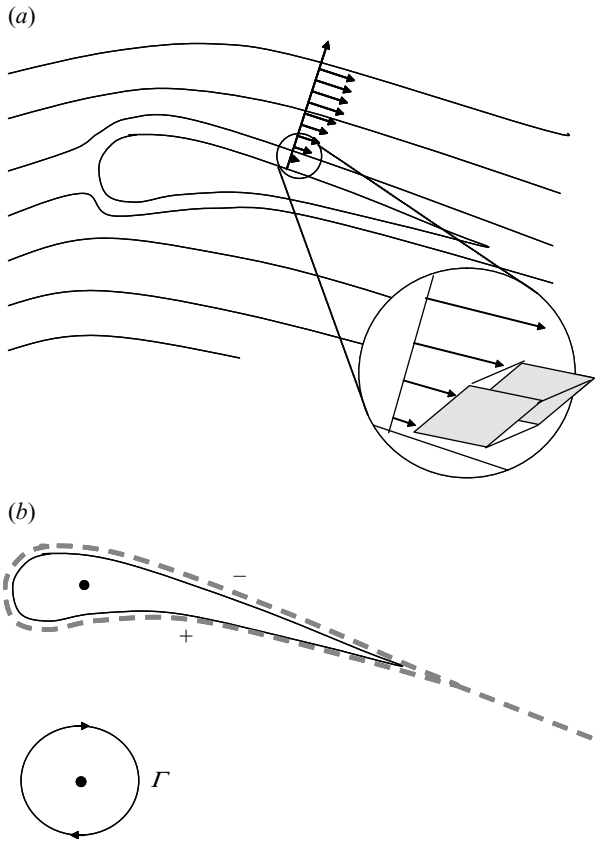

Figure 3. (*a*) When a streamlined shape such as an aerofoil at low angle of attack is placed in a uniform steady flow, then strong velocity gradients are confined to a thin boundary layer close to the solid surface. (*b*) Conceptually, the effect of aerofoil can be modelled as two thin vortex sheets, which are immersed in otherwise irrotational (vorticity-free) fluid. Finally the system can be represented by a single point vortex with strength Γ.

(c) *Practical aerodynamics*

(i) *Mathematical and physical simplifications*

Progress in practical aerodynamics cannot await solutions, numerical or otherwise, of the NS equations. Rather, success was achieved through a series of dramatic simplifications, quite radical in scope and elegant in conception—certainly a worthy analogue of the 'vast emptiness, nothing holy' description of Zen painting! The historical development of modern aerodynamic analysis can be traced enjoyably in Anderson (1997). Only the principles will be sketched in outline here, as many textbooks (again, Anderson (1984), would be a good choice) cover the material in detail.

The first simplification comes from the realization that when a streamlined body is placed in a uniform flow field, most of the changes in velocity occur in a thin layer close to the body, as illustrated in figure 3*a*. At the solid body

surface, the flow must be stationary, as fluid molecules are brought to a halt by contact with the surface. Recalling the conceptual fluid element of figure 2, the comparative inability of a fluid to resist shear deformations results in strong shearing motions in the fluid elements immediately next to this stationary layer, as the outer layers are required to match the speed of the mean flow. The intermediate region where the adjustment occurs is narrow and contains all of the shearing motion. In most of the fluid, nothing happens. The dynamics of the interaction of the boundary layer with the solid body are sufficient to account for all the forces exerted by the fluid on the body, and hence by the body on the fluid.

The second dramatic series of simplifications accompanied the representation of local shear by mathematical objects known as vortex elements, and on the development of the circulatory theory of lift generation, where the forces acting on the aerofoil can be formulated directly according to the strength of the vortex sheet representation, shown in figure 3*b*. In flows where shearing is confined to local regions, these regions can be represented by collections of vortex lines, or thin sheets which are embedded in an otherwise irrotational flow. In the two-dimensional aerofoil example of figure 3, the action of the aerofoil is modelled by the action of two thin, opposite-signed vortex sheets. In turn, these can be replaced by a single point vortex, with circulation, Γ, whose magnitude is proportional to the strength of the shear in the boundary layers. For small angles of attack, α, increasing α increases the downward deflection of the airstream, whose effect can be modelled as an increase in Γ. For small α, when the flow follows the aerofoil shape quite closely, remaining attached to the upper surface, all of the shear stresses occur inside the boundary layer, and the vertical component of the resultant force (per unit span) is

$$L' = \rho V \Gamma. \tag{3.12}$$

This is a stunning simplification of the full equations of motion of the fluid, giving (correctly) the magnitude of an important force component (weight of aircraft + load that can be supported in steady level flight) as a function of only three variables. The actual value of Γ, and its distribution over the span of a finite wing is a slightly more complicated calculation, but for certain assumed profiles of $\Gamma(y)$, simple analytical expressions can be derived for induced drag owing to lift, D_i. The force components are usually normalized with respect to the freestream dynamic pressure

$$q = \tfrac{1}{2}\rho V^2,$$

and S, a reference wing planform area, and so the force coefficients are expressed as,

$$C_{\mathrm{L}} = \frac{L}{qS} \quad C_{\mathrm{D}} = \frac{D}{qS}, \tag{3.13}$$

where the second expression for C_{D} is left general, rather than specific for D_i, the only component we have noted thus far.

Recalling the result from the dimensional analysis in § 3b, that dynamical similarity is assured for constant values of the Reynolds number, Re, then it is clear for a given aerofoil shape, the force coefficients can be functions of only two parameters

$$C_{\mathrm{L}},\, C_{\mathrm{D}} = f(Re,\ \alpha). \tag{3.14}$$

Again, this is a most extraordinary simplification of great practical significance. The lifting performance and fuel economy of an aerofoil depend on only two control parameters. Practical engineering tests are thus reduced to a finite number and the results can be considered complete for each shape.

Thin aerofoil theory, where wing sections can be replaced by vortex sheets, also allows an analytical prediction for how the performance should vary with α. The lift coefficient per unit span, c_{L}, is

$$c_{\mathrm{L}} = 2\pi\alpha, \tag{3.15}$$

again, an extraordinarily simple expression. Apparently c_{L} increases without limit as α increases. However, at some finite α (such as 10 degrees), the initial assumptions of the analysis are violated, the flow separates from the upper surface of the aerofoil, and in practice, the lift drops sharply.

(ii) *When do models work?*

Much has been written about when and whether equations such as equations (3.12)–(3.15) can be applied to the indubitably more complex situation of animal flight (e.g. Ellington 1984) or swimming, and we will not add to those words here. The purpose rather is to point out how far these simple algebraic expressions have come, from the original nonlinear partial differential NS equations (equation (3.6)). To get here, we had to make various model assumptions at different degrees of detail. The NS equations are already a model, requiring equation (3.3) to hold. The mathematical theorems and advances in practical aerodynamics by Lanchester, Prandtl, Helmholtz, Kutta and Joukowsky that propelled us through equations (3.12)–(3.15) add further layers of assumptions, based on physical reasoning, experimental observation and mathematical necessity. These are the powerful tools of aerodynamics that can be brought to bear on practical problems. They work very well, when the key simplifications work—when the flow can be modelled by a collection of vortex lines or sheets, immersed in an otherwise uniform irrotational flow. Much of the art of fluid mechanics experimentation is in enforcing or identifying similar concentrations of vortex lines, or their absence. In so doing, it is important to avoid the temptation for purportedly independent experimental tests to share the same fundamental assumptions of the models under scrutiny. For example, if the shedding of vortex rings is predicted behind some self-propelling device then they will be searched for and extracted from the mass of complicated swirling patterns in the flow. But what else is there? And does it matter?

4. COMPARING EXPERIMENT WITH THEORY

There are some principles concerning the comparison of experiment with theory that frequently go unremarked. Here, we pause to note them in a brief summary of a recent paper on the subject (Spedding & Pennycuick 2001).

(a) *Uncertainty analysis*

Much of science and engineering can be reduced (Zen-like) to the comparison of numbers. In particular we wish to determine the truth or falsehood of the proposition

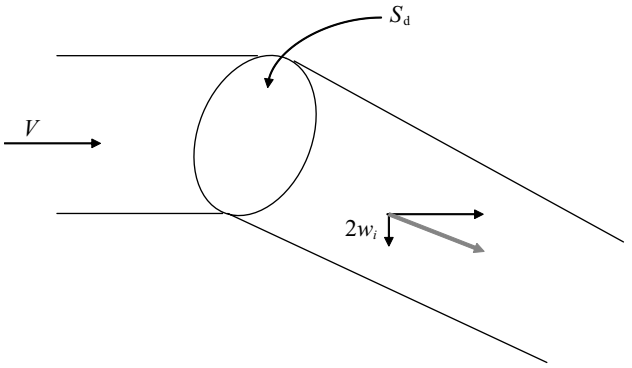

Figure 4. An actuator disc model for weight support in a flying bird. The bird itself is completely replaced by an imaginary disc of area $S_d = \pi b^2/4$, which acts like a lossless deflector, imparting sufficient downward momentum to the incoming air to support the weight, W.

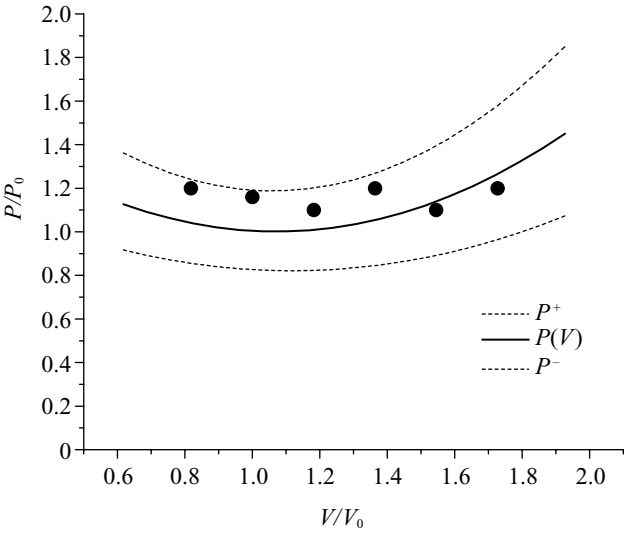

Figure 5. Total mechanical power, P, required for powered flight at speed V for a teal with weight, $W = 2.3$ N, and wing span, $b = 0.58$ m. P is normalized by its value at the minimum power speed, V_0. The familiar $P(V)$ curve is accompanied by upper and lower bounds represented by dashed lines, calculated from realistic values of measurement uncertainties. The imagined data points in grey circles might, by themselves, suggest a flat or odd-shaped power curve. As they all lie within reasonable uncertainty limits, however, no such inference can be made. Data and calculations from Spedding & Pennycuick (2001).

$$x_i = x_j \,. \tag{4.1}$$

If x_i and x_j are real, as is usually the case for physical quantities, then the probability of their having exactly the same value is vanishingly small, and so an unqualified answer is unobtainable. If, and only if, there are quantitative estimates of the expected variation in x_i and x_j, can the truth of the alternative proposition

$$x_i \pm \Delta x_i = x_j \pm \Delta x_j \tag{4.2}$$

be tested. The point is obvious, but not trivial, and becomes essential when more complicated cases involving more than one parameter are involved. What follows is a summary of how to compare numbers that are functions of more than one variable. Let y be a continuous function of n independent variables, $x_1, x_2, \ldots, x_n$

$$y = f(x_1, x_2, \ldots, x_n). \tag{4.3}$$

When the x_i variables are given small increments, then the change in y can be calculated exactly from

$$\Delta y = f(x_1 + \Delta x_1, x_2 + \Delta x_2, \ldots, x_n + \Delta x_n) - f(x_1, x_2, \ldots, x_n) = \Delta f. \tag{4.4}$$

In practice, it may not be clear how the Δx_i terms should be added so as to arrive at a reasonable estimation of their combined or individual effect, and we look for an analytical expression for Δf. A Taylor series expansion of equation (4.4) can be written

$$\Delta f = \frac{\partial f}{\partial x_1}\Delta x_1 + \frac{\partial f}{\partial x_2}\Delta x_2 + \ldots + \frac{\partial f}{\partial x_n}\Delta x_n + \varepsilon_1 \Delta x_1^m + \varepsilon_2 \Delta x_2^m + \ldots + \varepsilon_n \Delta x_n^m, \tag{4.5}$$

where the ε_i are small coefficients for higher-order terms whose magnitudes approach zero as Δx_i approaches zero. Thus, for small Δx_i,

$$\Delta f = \frac{\partial f}{\partial x_1}\Delta x_1 + \frac{\partial f}{\partial x_2}\Delta x_2 + \ldots + \frac{\partial f}{\partial x_n}\Delta x_n \tag{4.6}$$

is the total differential of f, and it gives the variation in f for small variations in one or more of its independent parameters. These variations can come from the inevitable nonzero uncertainties of experimental measurements, or they can represent a natural variation in the value of the parameter itself, when equation (4.6) acts as a compact representation for a sensitivity analysis. If the purpose of the calculation is to estimate uncertainties from experimental measurements, or from theoretical predictions based on empirical numerical estimates, then as the way in which the signed Δx_i values add is not known, the most likely uncertainty is calculated as

$$\overline{\Delta f} = \left\{ \left(\frac{\partial f}{\partial x_1}\overline{\Delta x_1} \right)^2 + \left(\frac{\partial f}{\partial x_2}\overline{\Delta x_2} \right)^2 + \ldots + \left(\frac{\partial f}{\partial x_n}\overline{\Delta x_n} \right)^2 \right\}^{\frac{1}{2}}. \tag{4.7}$$

$\overline{\Delta f}$ is the magnitude of the resultant vector whose independent orthogonal components are the Δx_i values. Typically, the Δx_i values come from single or multiple sample uncertainties of experimentally determined x_i values, and the function f is then differentiated, variable by variable, for each term. The procedure is frequently rather simple, depending somewhat on the form of f. In § 4b(i), an example where f is a real model function is used.

(b) *An example from a bird flight model*

(i) *The actuator disc*

The actuator disc model is perhaps a biomechanical model par excellence. As shown in figure 4, the flying animal is simply replaced as though the effect of its beating wings can be modelled by the action of a circular disc, which operates like a giant turning vane. Its sole function is to deflect air downwards, imparting a vertical velocity component to the uniform, initially horizontal flow. The equivalence of rate of change of momentum in the fluid with force has already been identified as an expression of Newton's laws in equation (3.5), and as the fluid is accelerating downward, the reaction force is upward. More detailed arguments concerning the physical basis for actuator disc models of various kinds can be found in standard

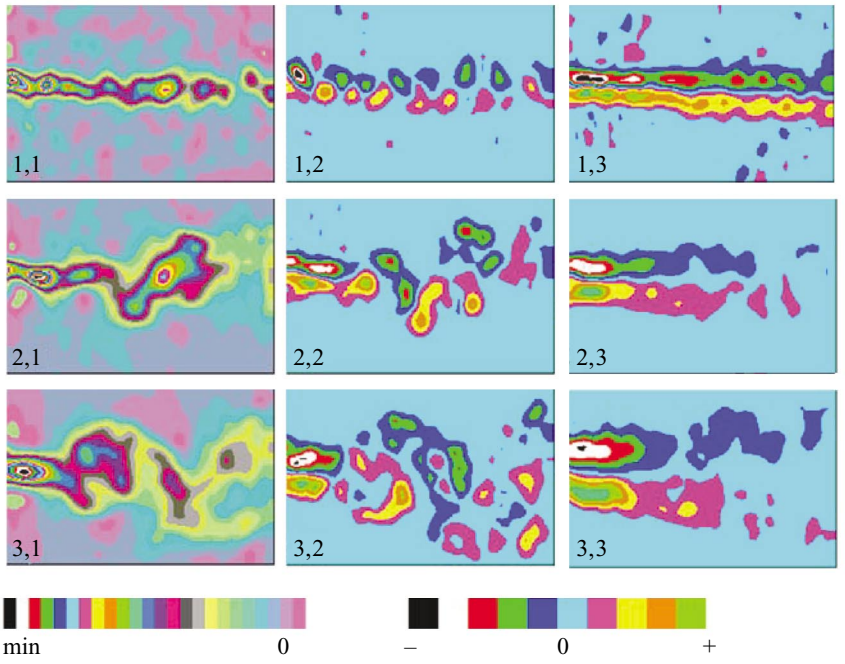

Figure 6. Vertical cross sections through the wake of a fixed rectangular wing of aspect ratio, AR = 3.4, fineness ratio, FR = c/h = 8.3 and $Re = 2.9 \times 10^4$. The panels are identified in {row, column} order. Each panel is of size $\Delta X/c = 3.85$, $\Delta Y/c = 2.36$, where $c = 5.07$ cm is the chord length. The $\{x, y\}$ coordinate system for the plane, with z perpendicular to it, is adopted for consistency with the notation of figure 2. The colour maps are from a 56×37 grid, and so each element is almost square with resolution $\delta x/c$, $\delta y/c = \{0.07, 0.065\}$. The aerofoil trailing edge is just upstream, beyond the left margin. The three rows from top to bottom represent different angles of attack, $\alpha = 2.3$, 11.6 and 20.1°. The three columns show the disturbance velocity field, $u(x, y)$ (in a reference frame moving with the mean flow speed, $U = 8.6$ m s^{-1}), the cross stream or spanwise vorticity, $\omega_z(x, y)$, and the time-averaged spanwise vorticity from 20 independent frames. The u and ω_z fields are shown on stepwise colour bars whose resolution reflects the uncertainty in the numerical values. There are 24 steps in u, and 10 in ω_z. The colour bars are scaled to local extrema at each α, where: $u_{\min} = [-2.7, -7.7, -12.6$ m s$^{-1}]$, $|\omega_z|_{\max} = [\pm 710, 880, 1270$ s$^{-1}]$ and $|\overline{\omega_z}|_{\max} = [210, 895, 895$ s$^{-1}]$.

aerodynamic texts (also Ellington 1984). Interestingly, almost regardless of the starting point of the analysis, one arrives at an expression for the induced power requirement as

$$P_i = \frac{2kW^2}{\rho V \pi b^2}, \tag{4.8}$$

where the animal moving through a fluid of density, ρ, at speed V, appears as a point mass with effective weight W, and wing/fin semispan b. By inspection, P_i is proportional to the weight, and inversely proportional to the mass flux through the disc of area $S_d = \pi(b/2)^2$. For a given speed, V, the only way to increase the mass flux (and so decrease P_i) is to increase S_d by increasing b. Alternatively, the animal must watch its weight. The crucial parameter in equation (4.8) is now seen to be the disk loading,

$$Q_d = \frac{W}{S_d}, \tag{4.9}$$

which completely controls the induced power requirement.

In this model, there are no wings, no tail flukes, no feathers, no wing veins, no elastic membranes, no kinematics, no wing geometry effects. All departures from the idealized case of uniformly accelerated downward flow are subsumed into the numerical value of k, a dimensionless coefficient whose value is greater than 1.

In the light of its obvious deficiencies, it may seem outrageous and/or primitive to persist in using a model like this. However, it is simple enough so that anyone can use it, program it and even modify it, and it is the only model for bird flight (for example) that has a large body of practical literature, freely available programs and estimates of required empirical constants (Pennycuick 1989).

(ii) *Uncertainty estimates*

It is quite common to see theoretical and even empirical curves of $P(V)$ in the animal locomotion literature, but very uncommon to see the curves bounded by bands of likely uncertainty. Here is how to remedy this problem for the particular case of equation (4.8).

In the language of equation (4.3), P_i is a function of five independent variables

$$P_i = f(k, W, \rho, V, b) \tag{4.10}$$

and so, following equation (4.6), we can write

$$\Delta P_i = \frac{\partial P_i}{\partial k}\Delta k + \frac{\partial P_i}{\partial W}\Delta W + \frac{\partial P_i}{\partial \rho}\Delta \rho + \frac{\partial P_i}{\partial V}\Delta V + \frac{\partial P_i}{\partial b}\Delta b. \tag{4.11}$$

Evaluating the partial derivatives gives

$$\Delta P_i = \frac{2W^2}{\rho V \pi b^2}\Delta k + \frac{4kW}{\rho V \pi b^2}\Delta W - \frac{2kW^2}{\rho^2 V \pi b^2}\Delta \rho - \frac{2kW^2}{\rho V^2 \pi b^2}\Delta V - \frac{kW^2}{\rho V \pi b^3}\Delta b, \tag{4.12}$$

which can be simplified to

$$\frac{\Delta P_i}{P_i} = \frac{\Delta k}{k} + \frac{2\Delta W}{W} - \frac{\Delta \rho}{\rho} - \frac{\Delta V}{V} - \frac{2\Delta b}{b}. \tag{4.13}$$

The most likely value for the uncertainty in P_i is

$$\overline{\Delta P_i} = P_i \left\{ \left(\frac{\overline{\Delta k}}{k}\right)^2 + \left(\frac{2\overline{\Delta W}}{W}\right)^2 + \left(\frac{\overline{\Delta \rho}}{\rho}\right)^2 + \left(\frac{\overline{\Delta V}}{V}\right)^2 + \left(\frac{2\overline{\Delta b}}{b}\right)^2 \right\}^{\frac{1}{2}}. \tag{4.14}$$

One advantage of performing this calculation is that the relative importance of accurate knowledge of certain terms can be quickly known by inspection; here, it is twice as important to know about the wingspan b and weight W than the remaining variables (including k).

(iii) *Quantitative results*

The procedure outlined for P_i can be followed in similar fashion for the remaining power components, and an expression for ΔP can then be formulated. The sensitivity to variations in W and b remains much higher than any of the other variables, as presaged in equation (4.14), and this fact can be immediately seen from the analysis without need for further numerical computation. The expressions for the uncertainties can be tracked through a numerical computation of the flight power curve, $P(V)$, however, and figure 5 shows a summary result.

The flight power curve now has two additional curves representing upper and lower bounds of $\pm \overline{\Delta P}(V)$ as computed from measured experimental uncertainties in a wind tunnel experiment. The expected variation in calculated mechanical power is a substantial fraction of the total change in power over the entire range of flight speeds. Consequently, a set of purely fictitious data points, scattered as shown on the same graph, might be interpreted by themselves as a refutation of either the specific flight power calculation values, or the shape of the power curve itself. They are not, because they are indistinguishable from the cloud of possible values given realistic experimental uncertainties for the numbers used in the theoretical calculation alone.

Some practical consequences are as follows.

(i) It is very difficult to perform a definitive laboratory experiment. Definitive field measurements are even harder.

(ii) The expected or likely variation of the computed power output, given realistic uncertainties of the contributing independent variables, is large compared with the predicted variation of P itself. There are therefore quite limited possibilities for making meaningful tests of either the particular shape of one model-predicted $P(V)$ curve, or of the relative merits of entirely different flight models.

(iii) A corollary of (ii) is that the construction of mechanical or aerodynamic models of greatly increased sophistication may not be justified, if the original objective (O in the introductory remarks) is restricted to making simple predictions of, say, flight speeds.

5. SAMPLE APPLICATIONS

The following examples are taken from recent research, selected to illustrate some of the general principles outlined here. The first is a seemingly simple and standard problem which reveals complexities in the flow field that contrast quite sharply with the rather idealized fluid flow models encountered so far. The second is from a nominally much harder problem, which also has some surprises. Both examples show data from wind tunnel experiments described further in Spedding *et al.* (2003*a*,*b*).

(a) *The wake of a fixed wing*

It is instructive to analyse the wake of a fixed rectangular wing in the same way as is commonly done for animal wakes, i.e. measuring the wake disturbance alone. For a given aerofoil shape (cross-sectional geometry and aspect ratio), steady flow solutions are a function of two parameters only

$$\boldsymbol{u}(\boldsymbol{x}) = f(Re,\ \alpha), \tag{5.1}$$

and figure 6 shows a selection of flow field quantities for $\alpha \cong 2$, 12 and 20°, and $Re \cong 3 \times 10^4$. The left-hand column shows the streamwise velocity component, u, in the frame of reference moving with the mean flow. The mean wake defect thus flows from right to left. In the top left, the wake for the lowest angle of attack, $\alpha \cong 2^\circ$, already differs markedly from the thin straight vortex sheet drawn schematically in figure 3. The wake itself is unstable, and wavy disturbances grow in amplitude eventually breaking up the wake towards the downstream end (right side of the panel). The cross-stream vorticity, ω_z (middle top, or $\{1, 2\}$), given by

$$\omega_z = \frac{\partial v}{\partial x} - \frac{\partial u}{\partial y}, \tag{5.2}$$

shows that the spatial modulation is always present and the vortex wake never appears as a flat thin sheet. The time-averaged vortex wake (top right, $\{1, 3\}$) does look more similar to the textbook pictures, but loses coherence towards the right-hand side, and no single instantaneous view corresponds to this.

At $\alpha \cong 12^\circ$ (row 2), the aerofoil is just below stall, the initial wake defect is still quite limited in the vertical direction, but becomes quite disorganized with increasing distance downstream. Likewise, the cross-stream vorticity is rather complex in structure, and at no instant does it correspond to the time-averaged value, whose decay with increasing x is increasingly evident. Beyond stall, at $\alpha \cong 20^\circ$ (row 3), the far wake structure is not qualitatively so different from the previous α, but the near wake, immediately behind the aerofoil, has increased in height. The instantaneous vortex wake $\{3, 2\}$ is quite spread out and intermittent. The time-averaged signal $\{3, 3\}$ is spread out vertically owing to the spatial and temporal intermittency.

A more detailed quantitative analysis of the rectangular wing wake is given in Spedding *et al.* (2003*a*). Here, we show only the drag coefficient as computed from integrating the wake defect profile (figure 7). Two sets of symbols are given, one for calculations from the time-averaged wakes, and one for the average of the sum of profiles through instantaneous wake structures. As the wake itself becomes more unsteady (the wake structure varies in both

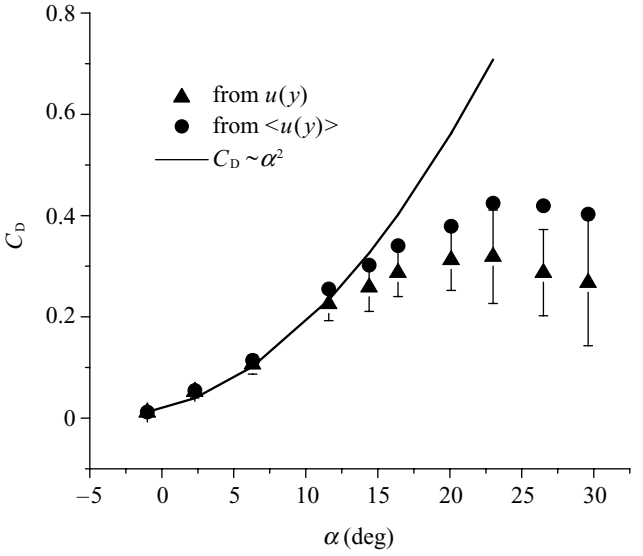

Figure 7. The drag coefficient on a rectangular wing as calculated from the wake momentum defect in data such as figure 6. The triangles are average values taken from $u(y)$ profiles in 20 instantaneous flow fields. The error bars show the standard deviation over the 20 velocity fields. The circles are calculated from time-averaged velocity profiles, $\overline{u}(y)$. The curve is a second-order polynomial fit to the mean values over the first four data points, and its extrapolation shows how a continued quadratic dependence of $C_D(\alpha)$ would appear. Redrawn from Spedding *et al.* (2003*a*).

space and time in unpredictable ways as hinted at in column 2 of figure 6), it is increasingly difficult to match calculations from the two, although the upper bound of the large variance in the instantaneous measure overlaps the mean value for most values of α. In both cases, the measured drag begins to deviate from an expected quadratic dependence on increasing α (illustrated by the solid curve in figure 7). The difference becomes significant after 15°, after stall, and when the wake structure becomes more complex (row 3 in figure 6), and the magnitude of three-dimensional disturbances (flow in the spanwise direction owing to instabilities and/or end effects) increases.

Based on the wake survey of the fixed wing, one must expect wake vorticity distributions to be significantly more complicated than simple theories would predict, even when the geometry and incoming flow field are very simple. This increased complexity and departure from ideal model conditions may or may not be important. Apparently reasonable drag coefficients can be calculated even when the flow structure appears as in row 2 of figure 6—not very similar to a flat vortex sheet. However, by the time we reach row 3 in this figure (qualitatively not extraordinarily different from row 2), the calculated drag coefficients do not agree with simple extrapolations from the lower α result, and it is clear from this and from the increase in variance in this measure that estimating forces from such unsteady and three-dimensional wakes is not simple.

Informed by the simple(!) model case, we can briefly examine similar data from a flapping bird.

(b) *The wake of a flying bird*

Figure 8 shows a combined velocity and vorticity field plot of a bird wake measured under similar circumstances as the aerofoil experiments. There are two patches of concentrated vorticity, and then in this view, little else. Helmholtz's laws require that vortex lines connect up in closed loops or end at a surface, and so with no nearby surface available (the wing semispan, $b = 12.6$ cm, and the smallest wind tunnel test section diameter, $d_{min} = 1.08$ m, so $(b/d)_{max} = 0.12$), the evidence seems quite good for the existence of simple closed loops in the bird wake. Thus, a single closed-loop wake model might well be a quite reasonable first-order approximation. The starting vortex on the right of figure 8 in particular is very compact and well defined. However, as the colour bar clearly shows, there is a strong asymmetry in the peak vorticity levels of the two vortex cross sections. The core cross section of the structure left at the end of the downstroke (left-hand side of figure 8) is less than 1/3 the peak magnitude of its opposite-signed counterpart. The precise arrangement of vortex lines therefore cannot be in a simple loop, and either some circulation must be left on the wing during the upstroke (i.e. it is aerodynamically active and vortex lines continue up into this part of the wake) or all the vortex lines do connect following the downstroke, but in a much more diffuse and disorganized way. Recall that the very notion of a vortex line is a mathematical one, useful for modelling fluid flows when the vorticity distribution is concentrated into discrete patches. The physical/empirical description of the wake structure need not mindlessly parrot this same formula. Recall also that, even though the wake structure may not look exactly like a simple ring structure, this might nevertheless continue to be a useful and convenient model description.

6. CONCLUDING REMARKS

This highly selective comparison of theoretical and experimental models in fluid mechanics has used two practical examples from recent experimental wind tunnel work to illustrate the advantages and difficulties of making model comparisons. The simple fixed aerofoil example showed that observed departures from theoretical model wake vorticity distributions may be important or unimportant, and it is not immediately obvious, *a priori*, which will be the case. So it is with the typically more complex problems in fluid mechanics modelling of animal locomotion. A model might be perfectly successful, even while details are being soundly refuted by physical experiments. Recall how the success or failure depends only on explicitly defined objectives, *O*, and these are not necessarily bound by the known physics, *P*. If it is convenient to pretend, for example, that all bird wakes are made of closed vortex loops, then one can do so. By the same token, of course, if it is convenient to continue to imagine a continuous tube of uniformly accelerated fluid, as in the actuator disc, one can also do this. The critical remaining component lies in the falsifiability of the model predictions. Critical and unambiguous tests can only be performed if, in addition to predicted numerical values or parametric curves, there are realistic estimates of the uncertainty. These uncertainty limits are themselves quite informative as to the expected precision of the outcome of a particular test, and as to the relative contribution from increased levels of complexity and/or realism in a model.

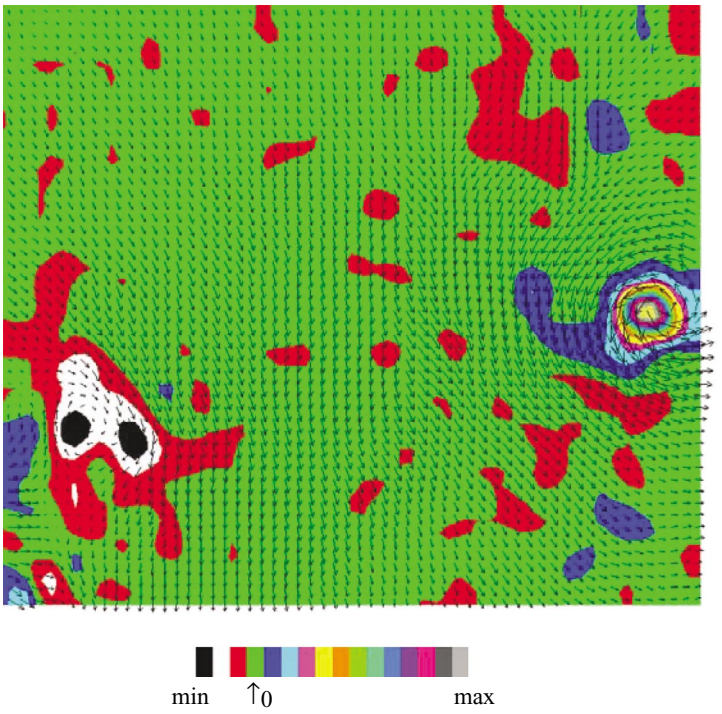

Figure 8. The wake of a thrush nightingale in steady level flight at 5 m s^{-1}, measured in a wind tunnel. As in the aerofoil experiments (figure 6), the reference frame moves with the mean flow speed, and the flow is as if the bird has passed from right to left, through still air. The cross-stream vorticity, $\omega_z(x, y)$, measured in a vertical centreplane is mapped onto a 16-step colour bar. The velocity vectors show qualitatively the flow field and the spatial resolution. The image size is *ca.* 20 cm × 18 cm, and the structure left behind on one downstroke fills the field of view. The maximum and minimum ω_z values are 980 and −290 s^{-1}, respectively. The Reynolds number based on mean chord, $Re_c = 1.5 \times 10^4$. From experiments and data described in Spedding *et al.* (2003*a*,*b*).

Many fluid mechanics problems are still regarded as difficult, partly because of the complexity of possible solutions to the Navier–Stokes governing equations. Consequently, the field has a noble history of ingenious and elegant simplified model problems that allow practical progress to be made in real problems. In parallel, experimental modelling has played a particularly important role, because provided the appropriate dimensionless numbers are matched (typically a Reynolds number), then physical experiments can be arranged with real fluids, where the fluid dynamics modelling then comes for free. The principal difficulty frequently arises in making independent and correct interpretations of the possibly complex flow solutions that one generates in the physical model. We can eagerly anticipate strong future progress on both sides of the equation.

ENDNOTES

[1]A famous story relates how, in the mid-sixteenth century, on being granted a coveted audience with the Emperor of China, Daruma, the first patriarch of Zen Buddhism, was asked for the most important principle of the rapidly growing religion. 'Vast emptiness, nothing holy!', exclaimed Daruma, by way of response. The Emperor, somewhat perplexed, demanded 'Who are you?' 'I do not know!' replied Daruma, who then promptly left and spent the next 9 years in meditation facing a wall. Daruma's outburst, 'Vast emptiness, nothing holy!' is quite a good means for recalling the important selection and omission process in model-making, and in ensuring that no examples are considered above criticism.

[2]This is a slight over-simplification, but it suffices for the current discussion and remains a good rule of thumb for quick estimates and analysis.

REFERENCES

Alexander, R. McN. 2003 Modelling approaches in biomechanics. *Phil. Trans. R. Soc. Lond.* B **358**, 1429–1435. (DOI 10.1098/rstb.2003.1336.)

Anderson, J. D. 1984 *Fundamentals of aerodynamics*. New York: McGraw-Hill.

Anderson, J. D. 1997 *A history of aerodynamics*. Cambridge University Press.

Ellington, C. P. E. 1984 The aerodynamics of hovering insect flight. Part V. A vortex theory. *Phil. Trans. R. Soc. Lond.* B **305**, 115–144.

Pennycuick, C. J. 1989 *Bird flight performance: a practical calculation manual*. Oxford University Press.

Pennycuick, C. J. 1992 *Newton rules biology: a physical approach to biological problems*. Oxford University Press.

Popper, K. R. 1959 *The logic of scientific discovery*. London: Hutchinson.

Spedding, G. R. & Pennycuick, C. J. 2001 Uncertainty analysis for experimental and theoretical power curves. *J. Theor. Biol.* **208**, 127–139.

Spedding, G. R., Hedenstrom, A. & Rosen, M. 2003*a* Quantitative studies of the wakes of freely-flying birds in a low-turbulence wind tunnel. *Exp. Fluids* **34**, 291–303.

Spedding, G. R., Rosen, M. & Hedenstrom, A. 2003*b* A family of vortex wakes generated by a thrush nightingale in free flight in a wind tunnel over its entire natural range of flight speeds. *J. Exp. Biol.* **206**, 2313–2344.

GLOSSARY

DNS: direct numerical simulation
NS: Navier–Stokes